

The deformation field in semiflexible networks

Alex J Levine^{1,3}, D A Head² and F C MacKintosh²

¹ Department of Physics, University of Massachusetts, Amherst, Amherst MA 01003-9300, USA

² Department of Physics and Astronomy, Vrije Universiteit, Amsterdam, The Netherlands

E-mail: levine@physics.umass.edu

Received 29 September 2003

Published 21 May 2004

Online at stacks.iop.org/JPhysCM/16/S2079

DOI: 10.1088/0953-8984/16/22/006

Abstract

Gels composed of semiflexible polymers have remarkably complex deformational properties. Due to the introduction of a new mesoscopic length scale, the persistence length, the deformation field of these materials can depart from the predictions of continuum elastic theories over mesoscopic lengths. In this paper, we review a recently proposed phase diagram for such semiflexible gels and discuss the implications of this research for modelling the cytoskeleton.

(Some figures in this article are in colour only in the electronic version)

1. Introduction

1.1. Flexible versus semiflexible gels and the cytoskeleton

Gels constituted from semiflexible polymers have qualitatively different elastic properties over mesoscopic length scales than gels constructed from flexible polymers. The underlying cause of this difference is that in the semiflexible gel, there is a new, mesoscopic length scale set by the persistence length of the filaments. For the gels considered here, the persistence length ℓ_p is generically larger than the filament length L , and the network mesh size or correlation length. In this case, we note that the static elastic moduli of the gel depend sensitively on the density of permanent cross-links, which in turn can differ substantially from the density of entanglements. As we show here, the moduli can also depend sensitively on the contour length L , or molecular weight. These results stand in contrast to the case of flexible polymers, in which the plateau modulus is essentially a function only of the density of entanglements [1, 2]. This difference reflects a principal distinction between the two chemical systems. In the semiflexible gel, the persistence length of the polymers ensures that each polymer chain at a permanent cross-link retains its chemical identity through that cross-link. In flexible gels, each piece of polymer between two cross-links can be considered to be an independent entity even though those polymer segments between different permanent cross-links may, in fact, be part of the same covalently bonded chain. It is only through the long-range correlation in chain tangent vectors

³ Author to whom any correspondence should be addressed.

imposed by the chain stiffness (alternatively the long persistence length) that the constituent elements of a semiflexible gel retain information on chemical identity from one cross-link to the next.

A second consequence of the long persistence length of the chains making up a semiflexible gel is that there are now two separate modes of elastic energy storage under deformation. The semiflexible chains must have an elastic bending energy in addition to the usual chain stretching energy. Thus, under an externally imposed deformation, the semiflexible gel stores energy in both bending and stretching modes of the chain. In contradistinction, a gel made of flexible polymers can store energy only in the stretching modes of the filaments. We will show that the relative partitioning of energy into bending and stretching modes is an important measure of how much the gel's deformation departs from the predictions of continuum elasticity over mesoscopic lengths.

It is important to note that semiflexible gels are ubiquitous materials—the cytoskeleton of eukaryotic cells is based primarily on a semiflexible, cross-linked gel constructed from actin filaments [3–7]. F-actin, or filamentous actin is a linear protein aggregate with a cross section of 7 nm and lengths under physiological conditions of 1–5 μm . These filaments are remarkably stiff having a thermal persistence length of 17 μm [8]. The semiflexible polymer network of the cytoskeleton is cross-linked by a large repertoire of actin binding proteins so that the mean distance between cross-links can be as small as 0.1 μm , a distance much shorter than either the typical filament length or the thermal persistence length. This network can be a highly nonequilibrium structure: actin filaments are continually polymerizing and depolymerizing while molecular motors (e.g. myosin) periodically apply localized stresses to various points within the living network. The biological significance of this chemically heterogeneous structure is that the cytoskeleton is the principal source of mechanical integrity of the cell. It is also a structure by which the cell both exerts stresses on its external environment and senses its local mechanical environment. The cytoskeleton is thus the primary agent involved in cellular structure, motility, and mechanosensory transduction. A quantitative theory for displacement and stress propagation through the cytoskeleton is then necessary to understand the general framework for cellular force generation and transduction [4, 9–11] that underlies such fundamental biological processes as cell division, motility [12], and adhesion [16, 14, 13, 15]. Understanding stress propagation in cells also has implications for the interpretation of intracellular microrheology experiments [17].

1.2. The model

In this paper we do not pursue this biophysical question in full detail, but rather examine a simple model for a semiflexible, cross-linked gel that nevertheless demonstrates some of the novel elastic properties of such networks. Our model system is a two-dimensional random network of monodisperse, semiflexible filaments that are permanently cross-linked at all crossing points. These cross-links are assumed to apply arbitrary constraint forces at the cross-link, but still allow the free rotation of the two filaments. Each filament has a stretching modulus μ and bending modulus κ so that the Hamiltonian of a filament is given by:

$$\mathcal{H} = \frac{1}{2}\kappa \int ds (\nabla^2 \mathbf{u})^2 + \frac{1}{2}\mu \int ds \left(\frac{dl}{ds} \right)^2 \quad (1)$$

where s is the arc length along the undeformed filament, $\mathbf{u}(s)$ is the transverse displacement of the filament, while $l(s)$ is the local extension/compression of that filament along its undeformed contour. See figure 1.

A gel composed of filaments obeying the above Hamiltonian was numerically constructed by laying down straight rods of length L in the two-dimensional simulation box with random

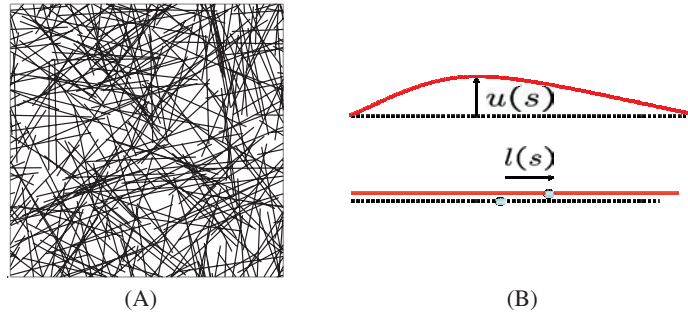


Figure 1. The left figure (A) is an example of a network with a cross-link density $L/\ell_c \approx 29.09$ in a shear cell of dimensions $W \times W$ and periodic boundary conditions in both directions. This example is small, $W = \frac{5}{2}L$; more typical sizes are $W = 5L$ to $20L$. The right figure (B) demonstrates the bending and stretching deformation of a single semiflexible filament. The solid red curve represents the deformed filament, while the dotted black curve is its undeformed contour.

centre positions and randomly distributed orientations. Wherever two rods crossed, they were permanently cross-linked; a network constructed in this manner has no initial strain energy. The sample with periodic boundary conditions was then subjected to uniform deformations via the Lees–Edwards method [18]⁴. Using a conjugate gradient method, we relaxed the system to its local energy minimum in this zero-temperature calculation.

For networks constructed in this manner there are three length scales. The first is L , the filament length. The second is ℓ_c , the mean distance between cross-links. This is the only measure needed to describe the isotropic random network. Since in two-dimensions there is a one-to-one mapping from cross-link density to filament density, this length also describes the filament concentration in the network. In three-dimensional generalizations of this model, however, ℓ_c will be related to the density of cross-linkers; for the sake of clarity we will refer to it in that manner while discussing our two-dimensional system as well. The final length scale in the problem is given by $\ell_b = \sqrt{\kappa/\mu}$, which is the length over which bends in the filaments relax, as can be shown from equation (1). For a macroscopic elastic rod, this is a length of the order of the radius a . Hereafter, we will discuss the system in terms of L , ℓ_c , and ℓ_b .

2. Results

2.1. Elastic energy and moduli

From the total elastic energy stored in the sample, one can determine the collective, zero-frequency elastic moduli of the system. Further numerical details can be found in [19–22]. Examples of the sheared network are shown in figure 2. From that figure it is apparent that there is a significant, qualitative change in the form of the elastic energy storage between the less dense network where the energy is stored primarily in the *bending modes* of the filaments ((A)—the left image) and the more dense network where the energy is stored in the *extensional/compressional modes* of the filaments ((B)—the right image). The reader may convince him/herself that for a network with freely rotating cross-links under affine deformation, one should expect that all the elastic energy would be stored in the extensional/compressional modes of the filaments (blue in figure 2). See inset of figure 3 as well. Thus, we see that upon change in cross-link density the network crosses over from a deformation regime inconsistent with the assumption of affine deformation where the energy is

⁴ The uniaxial strain γ_{yy} was imposed by allowing an infinitesimal gap between cell images in the y -direction, valid for our linearized, static networks [18].

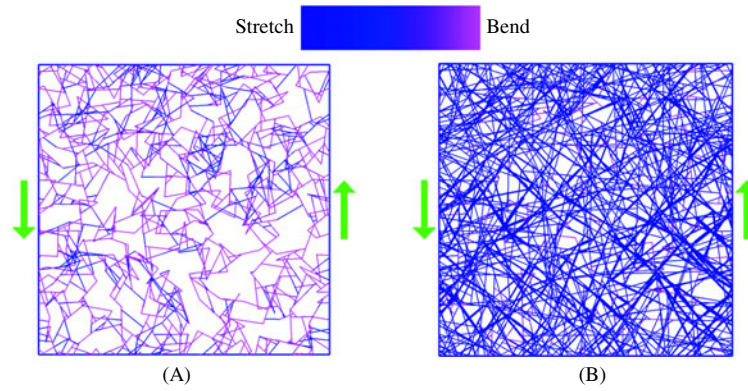


Figure 2. Examples of networks in mechanical equilibrium in the nonaffine (A) and affine (B) regimes. In both images the filament rigidity is $\ell_b/L = 0.006$, but in (A) $L/\ell_c = 8.99$, while in (B) $L/\ell_c = 46.77$. Dangling ends have been removed, and the thickness of each line is proportional to the energy density, with a minimum thickness so that all rods are visible (most lines in (a) take this minimum value). The calibration bar shows what proportion of the deformation energy in a filament segment is due to stretching or bending. Note the change in the partitioning of the elastic energy between stretching and bending modes between the two deformation regimes.

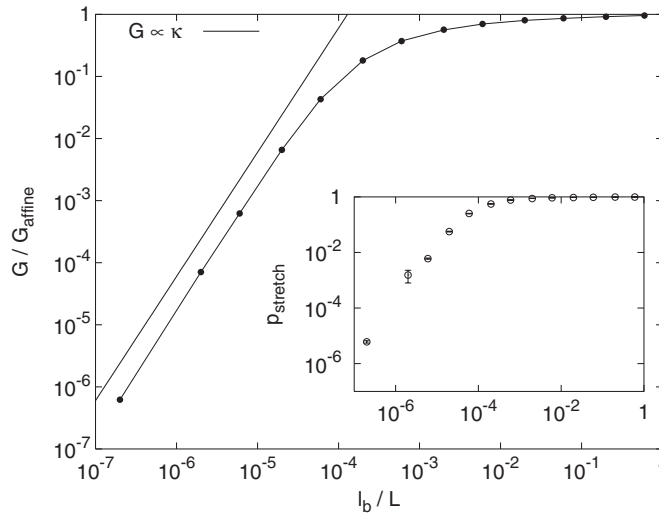


Figure 3. Shear modulus G versus filament rigidity ℓ_b/L for $L/\ell_c \approx 29.09$, where G has been scaled to the affine prediction for this density. The straight line corresponds to the bending-dominated regime with $G \propto \kappa$, which gives a line of slope 2 when plotted on these axes. Inset: the proportion of stretching energy to the total energy for the same networks, plotted against the same horizontal axis ℓ_b/L .

stored primarily in the bending of the filaments to a regime in which the filament deformation is almost entirely extensional/compressional, which is consistent with the assumption of affine deformation.

To further clarify this point, we examine the collective shear modulus of the network. The assumption of affine deformation allows one to calculate the static shear modulus of the network in terms of the extension modulus of the filaments:

$$G_{\text{affine}} = \frac{\pi}{16} \frac{\mu}{L} \left(\frac{L}{\ell_c} + 2 \frac{\ell_c}{L} - 3 \right). \quad (2)$$

We extract the shear modulus numerically and compare it with the value calculated above in figure 3. We see that the maximum modulus of the system is the affine value computed above. In addition, for the cases where the modulus departs significantly from its affine value, it scales as $G \sim \ell_b^2 \sim \kappa$ showing that the bending modes of the filaments dominate the elastic response function in the regime where the affine calculation dramatically fails [23]. If we assume (as will be demonstrated below) that the appearance of filament bending and the departure of the effective shear modulus from its affine value both signify a nonaffine deformation regime of the material, then the figures 2 and 3 taken together demonstrate two trends. The network becomes less affine when either: (i) the bending modulus decreases, or (ii) the density of cross-links decreases.

2.2. Affine versus nonaffine deformation

In order to discuss the properties of the deformation field for the various realizations of the network, one should not have to resort to energetics, but rather directly describe the geometry of the deformation. We wish to determine whether the deformation field is affine under uniformly imposed external deformations, by which we mean that it is self-averaging—all parts of the sample deformation in a manner identical to the whole. This self-averaging property may well be a function of length scale: the deformation field when suitably coarse-grained to a length g may have the self-averaging property, while it may not self-average when examined at a finer length scale, e.g. $g \rightarrow g/2$. At large enough scale the system must trivially self-average so that the sample will always be affine at the sample size. We introduce a measure of nonaffinity that is a function of length scale r , $\Xi(r)$. To define this scalar quantity, we note that it must be built from the deformation tensor, $\partial_i u_j$, where \mathbf{u} is the displacement field in the material. To distinguish nonaffine from affine deformations, one must look at the spatial gradients of this deformation tensor or compare it to a reference value computed for purely affine deformation. Numerically, it is more convenient to choose the latter. Finally, if we want a scalar quantity to define nonaffinity, we must consider the rotational invariants of the tensor. In two-dimensions, the deformation tensor may be decomposed into a scalar, a pseudoscalar, and a traceless symmetric tensor. Here we focus on the pseudoscalar part that may be interpreted as a local rotation angle. To be concrete, one may image painting lines of length g throughout the undeformed sample and then observe how these lines rotate under the imposed shear deformation $u_{ij}^{\text{affine}} = \hat{x}_i \hat{y}_j \gamma_0$. One may then compute the expected rotational angle under an affine deformation: $\Delta\theta^{\text{affine}} = -\gamma_0 \sin^2 \theta$, where θ is the angle that the undeformed line made with the \hat{x} -axis. We then define the degree of nonaffinity at the length scale g by a positive definite quantity which measures the difference between the observed and affine rotation angles:

$$\Xi(g) = (1/\gamma_0^2) \left\langle (\Delta\theta - \Delta\theta^{\text{affine}})^2 \right\rangle_g, \quad (3)$$

where the angled brackets, $\langle \rangle_g$ denote averaging over the sample of all lines of length g . From equation (3), it is clear that Ξ , being a positive definite quantity, will always have a nonzero average for any realization of the network. Due to the imposed affine deformation at the boundary of our sample, Ξ must go to zero at length scales approaching the system. There is, however, a nontrivial dependence of $\Xi(r)$ as r becomes small compared to the system size. We find that all networks examined fall into one of two broad categories with respect to the dependence of $\Xi(r)$ on length scale r . For networks that we will define as affine, $\Xi(r)$ grows with decreasing length scale but then plateaus at some finite value at length scales much larger than the mean distance between cross-links. In contrast, we observe that in the second class,

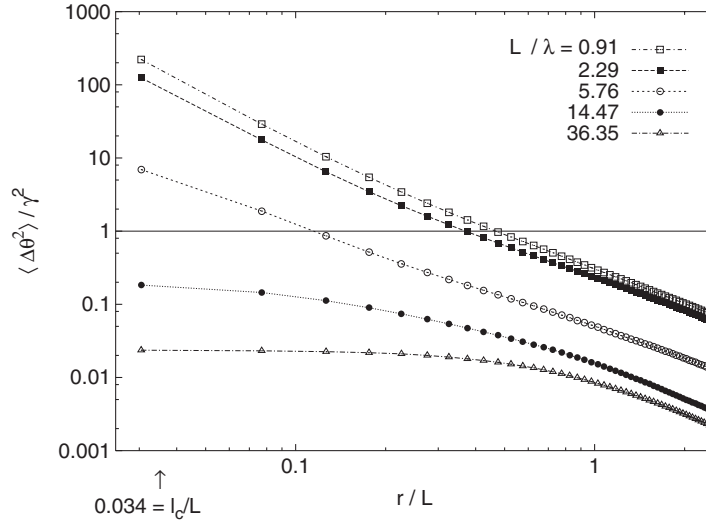


Figure 4. Plot of the affinity measure $\langle \Delta\theta^2(r) \rangle$ normalized to the magnitude of the imposed strain γ against distance r/L , for different ℓ_b/L . The value of r corresponding to the mean distance between cross-links ℓ_c is also indicated, as is the solid line $\frac{1}{\gamma^2} \langle \Delta\theta^2(r) \rangle = 1$, which separates affine from nonaffine networks to within an order of magnitude (the actual cross-over regime is somewhat broad). In all cases, $L/\ell_c \approx 29.1$ and the system size was $W = \frac{15}{2}L$.

which we call nonaffine, the measure of nonaffinity, $\Xi(r)$ grows monotonically as r decreases (see figure 4).

It is important to note that the two classes of networks (affine and nonaffine) can be differentiated by one criterion, the dimensionless ratio of the filament length L to a length λ is large compared to one for affine networks and small compared to one for nonaffine networks. We introduce and discuss this new length scale λ below.

3. The shear modulus and the deformation phase diagram

3.1. λ : a scaling argument

We now present a simple scaling argument to determine λ . We identify λ as the length along a filament over which the deformation is nonaffine. First we note that there are only two lengths in the problem to which we may compare L : ℓ_b, ℓ_c . Thus, we expect that λ can be written as

$$\lambda \sim \ell_c (\ell_c / \ell_b)^z. \quad (4)$$

It remains to determine the exponent z . To proceed, we note that the stretching-only solution presented above assumes that the stress is uniform along a filament until reaching the dangling end. It is more realistic to suppose that it vanishes smoothly. If the rod is very long, far from the ends and near the centre of the rod, it is stretched/compressed according to the macroscopic strain γ_0 . We assume that this decreases toward zero near the end, over a length l_{\parallel} , so that the reduction in stretch/compression energy is of order $\mu \gamma_0^2 l_{\parallel}$. The amplitude of the displacement along this segment, which is located near the ends of the rod is of order $d \sim \gamma_0 l_{\parallel}$. This deformation, however, clearly comes at the price of deformations of surrounding filaments, which we assume to be primarily bending in nature (the dominant constraints on this rod will be due to filaments crossing at a large angle). The typical amplitude of the induced

curvature is of order d/l_{\perp}^2 , where l_{\perp} characterizes the range over which the curved region of the crossing filaments extends. This represents what can be thought of as a bending correlation length, and it will be, in general, different from l_{\parallel} . The latter can also be thought of as a correlation length, specifically for the strain variations near free ends. We determine these lengths self-consistently as follows.

The corresponding total elastic energy contribution due to these coupled deformations is of order

$$\Delta E_1 = -\mu\gamma_0^2 l_{\parallel} + \kappa(\gamma_0 l_{\parallel}/l_{\perp}^2)^2 l_{\perp} (l_{\parallel}/\ell_c), \quad (5)$$

where the final ratio of l_{\parallel} to ℓ_c gives the typical number of constraining rods crossing this region of the filament in question. In simple physical terms, the rod can reduce its total elastic energy by having the strain near the free ends deviate from the otherwise affine, imposed strain field. In doing so, it results in a bending of other filaments to which it is coupled. From this, we expect that the range of the typical longitudinal displacement l_{\parallel} and transverse displacement l_{\perp} are related by

$$l_{\perp}^3 \sim \ell_b^2 l_{\parallel}^2 / \ell_c \quad (6)$$

in order to maximize the reduction in elastic energy ΔE_1 .

Of course, the bending of the other filaments will only occur because of constraints on them. Otherwise, they would simply translate in space. We assume that the transverse constraints on these bent filaments to be primarily due to compression/stretching of the rods which are linked to them. These distortions will be governed by the same physics as described above. In particular, the length scale of the corresponding deformations is of order l_{\parallel} , and they have a typical amplitude of d . Thus, the combined curvature and stretch energy is of order

$$\Delta E_2 = \mu\gamma_0^2 l_{\parallel} (l_{\perp}/\ell_c) + \kappa(\gamma_0 l_{\parallel}/l_{\perp}^2)^2 l_{\perp}, \quad (7)$$

where, in a similar way to the case above, l_{\perp}/ℓ_c determines the typical number of filaments constraining the bent one we focus on here. Minimizing ΔE_2 determines another relationship between the optimal bending and stretch correlation lengths, which implies:

$$l_{\perp}^4 \sim \ell_b^2 l_{\parallel} \ell_c. \quad (8)$$

Thus, the longitudinal strains of the filaments decay to zero over a length of order

$$l_{\parallel} \sim \ell_c (\ell_c/\ell_b)^{2/5}, \quad (9)$$

while the resulting bending of filaments extends over a distance of order

$$l_{\perp} \sim \ell_c (\ell_b/\ell_c)^{2/5}. \quad (10)$$

The physical implications of equations (9) and (10) is that a length of each filament of order l_{\parallel} experiences nonaffine deformation and this nonaffine deformation causes changes in the local strain field over a zone extending a perpendicular distance l_{\perp} from the ends of that filament. Thus when l_{\parallel} becomes comparable to the length of the filament, L , the network should deform in a nonaffine manner. We will refer to this length along the filament contour over which one expects to find nonaffine deformation as λ and we identify the mean-field prediction for the scaling exponent z in equation (4) as $z = 2/5$.

Since the ratio L/λ controls the degree of nonaffinity of the network, we expect that mechanical properties of the network also depend on this ratio. In particular, if one were to scale the shear modulus by the affine shear modulus (equation (2)) and the filament length by λ , one should expect all data to collapse onto a single master curve. This is indeed the case as shown in figure 5. From the optimization of this data collapse, we determine the scaling exponent, $z = 1/3$. The discrepancy between this result and our mean-field prediction is likely due to corrections to the naive scaling caused by the proximity of the second order critical point corresponding to rigidity percolation [24], which we have discussed further in [19].

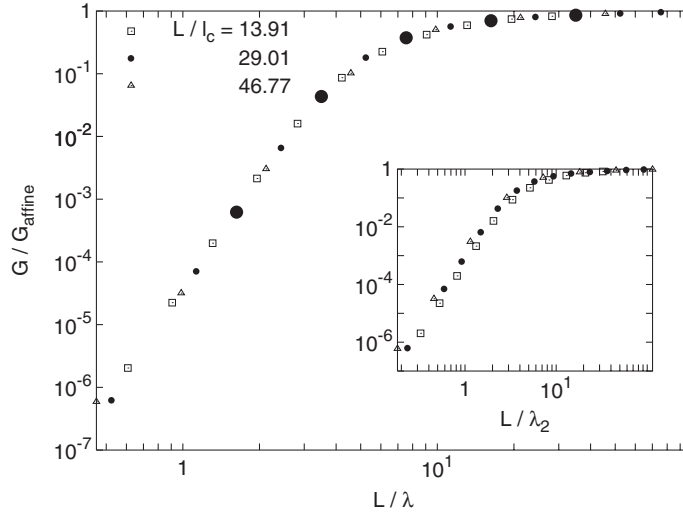


Figure 5. The master curve of G/G_{affine} plotted against L/λ with $\lambda = \ell_c(\ell_c/\ell_b)^{1/3}$ for different L/ℓ_c , showing good collapse. The enlarged points for $L/\ell_c \approx 29.09$ correspond to the same parameters as in figure 4. Inset: the same data plotted against L/λ_2 with $\lambda_2 = \ell_c(\ell_c/\ell_b)^{2/5}$, as predicted by the scaling argument in the text, showing slight but consistent deviations from collapse for this range of L/ℓ_c .

3.2. The phase diagram

The distinction which we draw between affine and nonaffine deformation regimes allows us to draw a phase diagram describing the entire range of possible deformation characteristics of semiflexible networks. The diagram is spanned by the independent axes of filament length L and cross-link concentration c . In addition to the cross-over between the affine (A) and nonaffine (NA) regimes, we include on the diagram a line of second order critical points corresponding to the rigidity percolation of the network. Below this solid line in figure 6 the material has no static shear modulus and is thus a solution. The dashed lines in the figure represent the cross-over in the gel (solid) phase of the material between the NA and A regimes. We emphasize that the NA \rightarrow A cross-over is not a thermodynamic phase transition like rigidity percolation. To complete the description of the phase diagram we note that there are, in reality, two different affine regimes depending on the network density and the bending modulus of the filaments.

To understand the appearance of the two different affine regimes: AE, the affine entropic regime, and AM, the affine mechanical regime, we note that the extension modulus of the filaments comes from two different sources. A semiflexible filament in thermal equilibrium has for entropic reasons a population of transverse fluctuations. These fluctuations store filament arc length which is recovered only under applied tension, which modifies the spectrum of these transverse oscillations. From such an analysis, originally discussed in [25], one computes the extension modulus to be

$$\mu_{\text{thermal}} = \kappa \ell_p / \ell^3 \quad (11)$$

where ℓ is the filament length and ℓ_p is the thermal persistence length. As the cross-link density increases, this extensional modulus related to the pulling out of transverse thermal fluctuations increases.

In addition to what we term the entropic or thermal modulus of the filament, there is also a mechanical modulus due to the actual change in the arc length of the rod. This modulus can

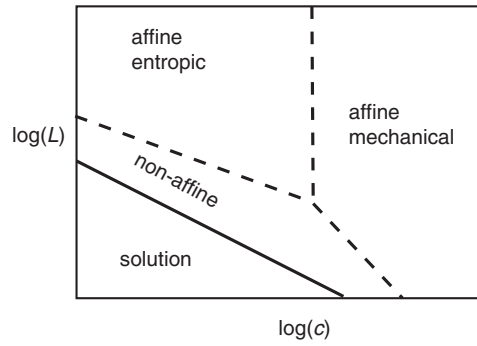


Figure 6. A sketch of the expected diagram showing the various elastic regimes in terms of molecular weight L and concentration $c \sim 1/l_c$. The solid line represents the rigidity percolation transition where rigidity first develops at a macroscopic level. This transition is given by $L \sim c^{-1}$. The other, dashed lines indicate cross-overs (not thermodynamic transitions), as described in the text. As sketched here, the cross-overs between nonaffine and affine regimes demonstrate the independent nature of these cross-overs from the rigidity percolation transition.

be estimated by assuming that the filament to be a homogeneous rod of cross-sectional radius a made up of a material that has Young's modulus Y_f . In that case the extensional modulus is given by: $\mu_{\text{mechanical}} = a^2 Y_f$. A comparison of the length dependent entropic modulus to the length independent mechanical modulus yields a critical distance between cross-links $l_* \sim (a^2 l_p)^{1/3}$. For $l_c < l_*$, the mechanical modulus is the smaller of the two moduli so that the compliance of the individual filaments is dominated by the actual stretching of the filaments and the network will be in the AM regime. If the cross-link density is lowered so that $l_c > l_*$, the extensional modulus will be primarily entropic in origin and the network will be in the AE regime. Since the network in both the AE and AM regimes deforms affinely, the linear mechanical response of the system is qualitatively similar. The nonlinear response to stress is nevertheless quite distinct since the entropic extension modulus is strongly strain-hardening as the population of transverse undulation modes is depleted under extension. The AM regime will not show such strongly nonlinear behaviour. Finally, no similar distinction need be made in the NA regime as the moduli of the network are controlled by the bending modulus of the rod. Here the shear modulus is generically much smaller than in the affine regimes and it should have a large linear response regime.

4. Biological implications

What are the implications of this analysis for the cytoskeleton? The phase diagram in figure 6 is generally applicable to all semiflexible networks; it remains to locate the F-actin network at physiological concentrations on this diagram. Firstly, we note that the thermal persistence length of F-actin is of the order of $10 \mu\text{m}$. For a cross-link density leading to $l_c \sim 200 \text{ nm}$, we find that the entropic modulus dominates the response of the individual filaments to applied tension. Thus, we find combining equations (11) and (4) that $\lambda \sim \sqrt{l_p l_c} \sim 1 \mu\text{m}$. Since typical cytoskeletal F-actin filaments have comparable lengths, we see that $L/\lambda \sim 1$ and these cytoskeletal networks are in the cross-over regime between the NA and AE regimes.

This result suggests that the cytoskeleton cannot be modelled as a continuum elastic object even at length scales of a few microns. We conclude that the theoretical study of force generation in and propagation through the cytoskeleton should not be based on a naive model of continuum, isotropic elasticity. Similarly, intracellular microrheological data should not be

analysed along such lines. In the broader view, one may wonder the why cytoskeletal network seems to be tuned to the cross-over between the NA and AE regimes. Although we have no way of knowing that such tuning was selected for in the evolutionary sense, we note that this cross-over region is a region in which small changes in λ (changed through local modifications in the cross-link density) lead to order of magnitude changes in the shear modulus—see figure 5. In addition, by tuning from the NA to AE regimes, the network shifts from having a large linear-response regime to a highly strain-hardening regime. Thus proximity to the cross-over does create a highly tunable system (both in terms of linear and nonlinear response) controlled by small modifications in the concentration of actin cross-linking proteins. Such mechanical/rheological tunability may also be highly desirable in biomimetic materials based on F-actin chemistry.

References

- [1] de Gennes P G 1979 *Scaling Concepts in Polymer Physics* (Ithaca, NY: Cornell University Press)
- Doi M and Edwards S F 1986 *Theory of Polymer Dynamics* (New York: Oxford University Press)
- [2] Rubenstein M and Colby R H 2003 *Polymer Physics* (London: Oxford University Press)
- [3] Alberts B, Bray D, Lewis J, Raff M, Roberts K and Watson J D 1994 *Molecular Biology of the Cell* (New York: Garland)
- Janmey P A 1991 *Curr. Opin. Cell Biol.* **3** 4
- [4] Elson E L 1988 *Annu. Rev. Biophys. Biochem.* **17** 397
- [5] Janmey P A, Hvidt S, Lamb J and Stossel T P 1990 *Nature* **345** 89
- [6] MacKintosh F C and Janmey P A 1997 *Curr. Opin. Solid State Mater. Sci.* **2** 350
- [7] Sackmann E 2002 *Physics of Biomolecules and Cells* ed H Flyvbjerg, F Jülucher, P Ormos and F David (Paris: Springer)
- [8] Gittes F, Mickey B, Nettleton J and Howard J 1993 *J. Cell Biol.* **120** 923
- Ott A, Magnasco M, Simon A and Libchaber A 1993 *Phys. Rev. E* **48** 1642(R)
- [9] Bohm J, MacKintosh F C, Shah J V, Laham L E, Janmey P A and Gluck J 1997 *Biophys. J.* **72** TU287
- [10] Wang N, Butler J P and Ingber D E 1993 *Science* **260** 1124
- [11] Stamenovic D and Wang N 2000 *J. Appl. Physiol.* **89** 2085
- [12] Stossel T P 1993 *Science* **260** 1086
- Stossel T P 1994 *Sci. Am.* **271** 54
- [13] Guttenberg Z, Lorz B, Sackmann E and Boulbitch A 2001 *Europhys. Lett.* **54** 826
- [14] Braun D and Fromherz P 1998 *Phys. Rev. Lett.* **81** 5241
- [15] Ralphs J R, Waggett A D and Benjamin M 2002 *Matrix Biol.* **21** 67
- [16] Mazia D, Schatten G and Sale W 1975 *J. Cell Biol.* **66** 198
- [17] Yamada S, Wirtz D and Kuo S C 2000 *Biophys. J.* **78** 1736
- Fabry B, Maksym G N, Butler J P, Glogauer M, Navajas D and Fredberg J J 2001 *Phys. Rev. Lett.* **87** 148102
- [18] Lees A W and Edwards S F 1972 *J. Phys. C: Solid State Phys.* **5** 1921
- [19] Head D A, MacKintosh F C and Levine A J 2003 *Phys. Rev. E* **68** 025101(R)
- [20] Head D A, Levine A J and MacKintosh F C 2003 *Phys. Rev. Lett.* **91** 108102
- [21] Wilhelm J and Frey E 2003 *Phys. Rev. Lett.* **91** 108103
- [22] Head D A, Levine A J and MacKintosh F C 2003 *Phys. Rev. E* **68** 061907
- [23] This bending dominated regime was identified by:
Kroy K and Frey E 1996 *Phys. Rev. Lett.* **77** 306
Frey E, Kroy K and Wilhelm J 1998 *Dynamical Networks in Physics and Biology* ed D Beysens and G Forgacs (Berlin: EDP Sciences–Springer)
- [24] For a review see
Sahimi M 1998 *Phys. Rep.* **306** 213
For rigidity percolation in the system discussed above see
Latva-Kokko M and Timonen J 2001 *Phys. Rev. E* **64** 066177 and [19]
- [25] MacKintosh F C, Käs J and Janmey P A 1995 *Phys. Rev. Lett.* **75** 4425